Growth allometry and dental topography in Upper Triassic conodonts support trophic differentiation and molar-like element function

Valentin Kelz[1], Pauline Guenser*[1], Manuel Rigo[2], Emilia Jarochowska[1, 3]

[1] Fachgruppe Paläoumwelt, GeoZentrum Nordbayern, Friedrich-Alexander-Universität Erlangen-Nürnberg, Erlangen, Germany. valentin.kelz@fau.de; pauline.guenser@gmail.com

[2] Department of Geosciences, University of Padova, Padova, Veneto, Italy. manuel.rigo@unipd.it

[3] Department of Earth Sciences, Utrecht University, Utrecht, Netherlands. e.b.jarochowska@uu.nl

*Corresponding Author

mailto: pauline.guenser@gmail.com

Abstract

Conodont elements are distinguished by their high morphological diversity and evolution, but their function has been few investigated. In particular, P_1 elements were proposed to be analogous to mammal molars based on a positive allometric relationship between their platform length/area and their total length, which was previously identified in Carboniferous taxa. Here we apply the same method to test the null hypothesis of isometric growth in two Late Triassic taxa, *Metapolygnathus communisti* and *Epigondolella rigoi*, using 3D models of growth series. We further test if these co-occurring taxa showed the same growth allometry, reflecting overlapping trophic niches. In both species platform length and platform area showed positive allometry with respect to element length, which is consistent with a molar-like function. The allometric relationship did not differ significantly between both Late Triassic taxa, which mean they rather occupy the same trophic niche. We further tested the overlap in the trophic niches using Dirichlet Normal Energy, a dental topographic analysis. Adult specimens of *E. rigoi* showed higher DNE values than *M. communisti*'s, consistent with a capacity to break harder food and so having a different diet. Based on DNE values available for primates, adult values for *E. rigoi* were similar to those reported for insectivores or folivores; for folivores or omnivores

for adults *M. communisti*. This means that these conodont species might have eaten food that required analogous breaking forces. Diet differentiation within this broad niche supports trophic diversification as an important driver of the remarkable disparity of conodont elements.

Introduction

Conodonts are extinct, eel-shaped marine animals that lived from the mid-Cambrian to Early Jurassic (Du et al. 2020). They are early vertebrates, either stem-gnathostomes (Donoghue et al. 1998) or stem-cyclostomes (Miyashita et al. 2019), and they distinguished by an extensive fossil record (Foote and Sepkoski 1999; Donoghue 2001*a*). The majority of the conodont fossil record consists of the phosphatic elements forming the feeding apparatus of the animal (Schmidt 1934; Scott 1934; Purnell et al. 2000). Conodont elements were retained throughout the life of an individual (Donoghue and Purnell 1999*a*), recording periodic growth through the apposition of crown tissue lamellae (Zhang et al. 1997; Dzik 2008). Soft tissues are rarely found and have, so far, not revealed a great diversity of body forms. Because of this, conodont taxonomy and functional morphology are based on their elements (Mazza et al. 2012*b* for the Upper Triassic and references therein). Patterns interpreted to be produced by elements shearing on the surface and repaired during the animal's growth suggest macrophagy (Purnell 1995; Donoghue and Purnell 1999*a*; Shirley et al. 2018). An active, predatory lifestyle is supported by the discovery of a conodont specimen with preserved extrinsic eye musculature (Gabbott et al. 1995), which was interpreted as indicative of conodonts having pattern vision (Purnell 1994). Calcium isotope analyses indicated that Late Devonian conodonts were first-level zooplanktivore and piscivore consumers (Balter et al. 2019), suggesting that in this period, conodonts did not live a purely predatory lifestyle. However, and despite several publications related to this topic, the diet of conodonts and its evolution is far from being resolved.

Conodonts changed their apparatus structure and disparity across their stratigraphic range (Dzik 1991, 2015), possibly reflecting their evolving niches as marine ecosystems increased in complexity (Klug et al. 2010; Ginot and Goudemand 2019). Under the assumption that conodont element morphology is an adaptation to their diet (Jones et al. 2012*a*; Ginot and Goudemand 2019; Guenser et al. 2019; Petryshen et al. 2020), the disparity suggests changing trophic position throughout the existence of the lineage. Calcium isotope analysis indicated that trophic niches overlapped, suggesting competition between some taxa (Balter et al. 2019). On the other

hand, Sr/Ca ratios in Silurian conodont assemblages indicate consistent differences between species (Terrill et al. 2022), possibly reflecting trophic niche differentiation through disruptive selection. Since there is no direct evidence of conodont food base, trophic diversity of conodonts must be inferred from proxies, e.g. by evaluating morphological and functional diversity of food-processing elements.

Several lines of argumentation have been proposed in support of elements of the conodont feeding apparatus having a tooth-like function. S and M elements, positioned in the anterior part, i.e. the mouth, are interpreted to perform a grasping function, whereas P elements, placed in the posterior part of the apparatus in the pharynx of the animal, have been proposed to have a function similar to molars of mammals (Purnell and von Bitter 1992; Purnell 1994; Donoghue and Purnell 1999*b*; Goudemand et al. 2011). A model of conodonts being suspension feeders has also been suggested (Nicoll 1987), where elements would be covered in tissue and S and M elements would filter particles and create current. P elements would only lightly mash food. This model, however, is not supported by more recent research: Shirley et al. (2018) suggested that tooth-like function in conodont elements may have only developed after a larval stage, during which they exhibited a different feeding habit, as mechanical wear of conodont elements is only present after a certain stage of ontogenetic development. After this stage, elements appear to have had prolonged intervals of dental use and short growth intervals, during which conodonts did not feed and their elements were covered in soft tissue, depositing new layers (Bengtson 1976; Donoghue and Purnell 1999*a*; Shirley et al. 2018).

The following arguments have been proposed for the dental function of conodont elements: (1) the presence of microwear patterns on conodont elements, produced *in vivo* (Purnell 1995; Martínez-Pérez et al. 2014*a*); (2) occlusion models (Donoghue and Purnell 1999*b*; Jones et al. 2012*a*; Martínez-Pérez et al. 2014*b*, *a*); (3) Finite Element Analysis (FEA) (Jones et al. 2012*b*; Martínez-Pérez et al. 2014*a*, 2016); (4) ultrastructural adaptation of conodont tissues to dental function, analogous to enamel (Donoghue 2001*b*; Jones et al. 2012*a*); (5) in some conodont taxa, extreme sharpness has been proposed to be an adaptation to cutting function in the absence of jaws acting as levers (Jones et al. 2012*b*); and the last argument, which is central in this study, (6) growth allometry (Purnell 1993, 1994).

Allometry describes proportional relationships of body parts, usually of the size of an organ to the total size of the organism. Proportional growth, whereby the growth of an organ and the size

of the animal increase at the same rate, is called isometry. Positive allometry then describes the organ growing at a higher rate than the rest of the animal. Negative allometry, conversely, describes the organ growing at a slower rate than the rest of the body (e.g., Gould 1966; Alberch et al. 1979; Klingenberg 1996). Tooth function is linked to surface area and the food requirements of an animal increase at a higher rate than an isometrically growing tooth (Gould 1966). For conodonts, positive allometric growth of elements would be expected if conodont elements had a tooth-like function, specifically if P_1 elements were used like molars. This hypothesis was first tested with Carboniferous *Idiognathodus* sp. and *Gnathodus bilineatus* conodont elements (Purnell, 1993, 1994). In these studies, the author assessed the molar function of P_1 elements by testing positive allometric growth patterns of their platform regarding the total length of the element since this part of P_1 elements was hypothesised to be an occlusal surface. As P_1 elements are paired, opposed platform surfaces would mash/ground food between them. Here, we apply a similar protocol applied by Purnell (1993, 1994) for assessing the dental function of two Late Triassic platform-bearing conodont species *Metapolygnathus communisti* Hayashi, 1968 (Hayashi 1968) and *Epigondolella rigoi* Kozur, 2007 (Noyan and Kozur 2007), which co-occurred in the studied area (Mazza et al. 2012*a*). We also add a dental topographic analysis, the Dirichlet Normal Energy (DNE), which measures the curvature and morphological irregularity of a surface. Essentially, DNE measures how much a given surface differs from a plane (Bunn et al. 2011). Surface topography is an important feature of teeth because they help break down food (i.e. the demand of energy) and can be used to infer diet (Bunn et al. 2011). Then, a particular DNE value of the occlusal surface of a teeth (or tooth-like buccal elements in conodonts) reflects a particular diets. In contrast to allometry, DNE is a new tool and has, until now, been only used to analyse skeletal parts of mammals, especially primate teeth (Bunn et al. 2011; Godfrey et al. 2012; Winchester et al. 2014; Prufrock et al. 2016; Berthaume and Schroer 2017; López-Torres et al. 2018; Pampush et al. 2019; Fulwood 2020; Li et al. 2020; Cuesta-Torralvo et al. 2021), but also marsupials (Lang et al. 2022), carnivorans (hyenas, bears) (Pérez-Ramos et al. 2020; de Vries et al. 2021; Lang et al. 2022), scandentians (tree shrews) (Selig et al. 2019), rodents (Prufrock et al. 2016; Renaud and Ledevin 2017; Vermeer 2019; de Vries et al. 2021), chiropters (Pellegrom 2019; López-Aguirre et al. 2022; Villalobos-Chaves and Santana 2022), multituberculates (Robson 2018), artiodactyls (suids) (Rannikko et al. 2020), eulipotyphles (hedgehogs) (Vitek et al. 2021) and one mammal stem group (Harper et al. 2019).

Moreover, only few of these authors used DNE values to directly infer animal's diet, most of them included DNE values in more complex multivariate analyses. Preliminary dental topographic analyses have been applied to conodont elements suggested that conodonts might have different diets through time (Purnell and Evans 2009; Stockey et al. 2021, 2022).

In this work, we address the hypothesis, originally tested by Purnell (1993), that conodont P_1 elements performed molar-like function and that this is reflected in the growth allometry of their surface *versus* length. The null hypothesis is that this relationship is isometric, what would be expected in filter feeders. In contrast to Purnell's (1993) study, which used projections of the surface on a plane, we use 3D meshes to calculate a more accurate platform area than is possible with a two-dimensional approximation. We further test the hypothesis that conodonts occupying the same environments had the same trophic position. To reject this hypothesis, slopes of the growth allometry of P_1 platform surface *versus* element length should differ. Under the assumption that P_1 platforms performed a molar-like function, we further hypothesise that the diets of studied species did not change during the ontogenetic growth of one species. This hypothesis is tested using DNE on platform elements, as most morphological variability between species is related to P_1 platform shape. Thus, platforms are inferred to reflect differences in their trophic positions (Jones et al. 2012*b*; Martínez-Pérez et al. 2016). Under the null hypothesis, DNE values are expected to increase with conodont size at the same rate. Differences in rates would suggest two possible explanations: (1) the diets changed across growth stages or (2) the energy demand of the two species changed at different rates during their ontogenies. Under the null hypothesis, the DNE values of the two species are expected to change at the same rate. Different rates of DNE increase across growth stages between the two species would falsify the hypothesis, indicating either a change of food base leading to different platform sharpness or a higher energy demand of the species with the higher rate of DNE increase.

Materials & Methods

Material

We studied two growth series of the ozarkodinid conodont species *Metapolygnathus communisti* and *Epigondolella rigoi* from the Pizzo Mondello section in western Sicily, Italy. They were collected from a section of 430 m thick marine limestone that is dated to the upper Carnian to upper Norian (Mazza et al. 2012*a*). Twenty-seven P_1 elements of *M. communisti* and

153 23 P_1 elements of *E. rigoi* were used, both separated into six growth stages (GS) based on the
154 maturity of morphological characters of the platform (Mazza and Martínez-Pérez 2015). The six
155 growth stages are GS1 – early juvenile, GS2 – juvenile, GS3 – late juvenile, GS4 – early adult,
156 GS5 – adult and GS6 – late adult (Mazza and Martínez-Pérez 2015) (Table 1). At Pizzo
157 Mondello, *M. communisti* occurs from the upper Carnian to the lower Norian (from c.a. -227.5
158 Ma to c.a. -226.5 Ma) (Mazza et al. 2012*a*, 2018; Ogg et al. 2020). The specimens range from
159 late juvenile to late adult (i.e., from GS3 to GS6), though mature elements are more abundant
160 (Table 1). The stratigraphic range of *E. rigoi* at Pizzo Mondello is from the lower Norian to the
161 middle Norian (from c.a. -227 Ma to c.a. -216 Ma) (Mazza et al. 2010, 2012*a*; Ogg et al. 2020), a
162 longer interval than *M. communisti*. Elements range from GS2 to GS5, earlier ontogenetic stages
163 are sparse (Table 1). These specimens have an average colour alteration index (CAI) of 1,
164 suggesting minimal post-depositional heating (Epstein et al. 1977; Nicora et al. 2007; Mazza et
165 al. 2012*a*). The studied elements are housed in the collection of the Dipartimento di Scienze
166 della Terra "A. Desio" of the Università degli Studi di Milano. The whole conodont collection
167 from the Pizzo Mondello section is housed in Milan and Padova (Department of Geosciences,
168 University of Padova).

169 **Methods**

170 ***Scanning***

171 The specimens were scanned with a resolution of 1 µm with a microtomograph nanotomS
172 (General Electric) of the AniRA-ImmOs platform, SFR Biosciences (UMS 3444), Ecole
173 Normale Supérieure de Lyon, France. Amira© software was used for the 3D reconstruction
174 (Guenser et al. 2019; **Figure 1**). The meshes are available on MorphoBank:
175 http://morphobank.org/permalink/?P4048

176 ***Growth allometry***

177 The length of the element was used as a proxy for the size of the conodont animal, as was
178 done in previous studies (Purnell 1993, 1994; Zhang et al. 2018; Ginot and Goudemand 2019).
179 The element length, the platform length and the platform area were measured using the 3D
180 software MeshLab (Cignoni et al. 2008). The length of the element was measured from the
181 anteriormost point of the blade in a straight line to the middle of the posterior edge of the
182 element's platform. As the platform is not equally long on the two sides of the blade, its length

was measured in two ways. First, as most elements are curved, the convex side of the platform was measured. In *Metapolygnathus communisti*, the convex size tends to be the longer side of the platform, though not always. In *Epigondolella rigoi* the convex side was almost exclusively the longer side. Alternatively, the longest side of the platform was measured, regardless of curvature (Figure 2, see also Figure S1 in Supplementary Information). In *M. communisti*, in both instances, the platform was measured from the most anterior part of the platform to its posterior end in a line parallel to the imagined symmetrical axis of the platform (Figure 2). In *E. rigoi*, the platform was measured from the geniculation point to the platform's posterior end. This measure was chosen because the anterior trough margin in this species, though reduced, reaches quite far up the blade, especially in more mature growth stages (see Mazza et al. 2012*a* for details about the taxonomic characters).

The measured area of the platform includes the platform, the cusp and any postcarinal nodes (Figure 2). In *M. communisti*, specimens of earlier growth stages tend to exhibit only one postcarinal node, already present in GS1 (Mazza and Martínez-Pérez 2015). From GS3 on, a second posterior node may appear (Mazza and Martínez-Pérez 2015). Adult specimens show three or four posterior carinal nodes (Mazza et al. 2012*a*). However, our measurements consistently included only two or three postcarinal nodes in adult specimens. In *E. rigoi*, the cusp is always followed by a single larger postcarinal node (Mazza et al. 2012*a*). These parts of P_1 elements were added to the measurements of the platform area, even though they are taxonomically not part of the platform, because they likely played a similar part in the processing of food as the platform itself. In *E. rigoi*, the anterior trough margin was not included in the measurements of the platform area (Figure 2). The anterior trough margin is not present in *M. communisti* (Mazza et al. 2012*a*).

Reduced major axis regression (RMA) was calculated using the R package "smatr" 3.4-8 (Warton et al. 2012; R Core Team 2021) to examine the relationship between the length of the platform and the length of the element, as well as the logarithm of the platform area and the length of the elements. The platform area was log-transformed to account for its increase as a square of the length of the element. RMA was chosen as a method because both variables are mutually dependent. Slopes obtained with *E. rigoi* and *M. communisti* data were compared with the "slope.com" function of the "smatr" R package. The same function was used to compare slopes related to the convex side and the longer side of the platform within a species. Slopes

between both species and isometry were compared with "slope.test" function of "smatr" R package. Isometry was modeled with a slope coefficient of 1 when testing the platform length *vs.* element length; a slope coefficient of 2 when testing the platform area *vs.* element length.

Purnell (1994) used a Z-test (Hayami and Matsukuma 1970) to test whether slope coefficients of *Idiognathodus* sp. and *Gnathodus bilineatus* differed significantly from isometric growth. A Z-index higher than 1.96 means that the relationship differs from isometry significantly. We consider this index comparable to the p-values we obtained for *M. communisti* and *E. rigoi* when comparing their slope coefficients with slopes expected under isometry. To compare slope coefficients from this study with those provided by Purnell (1994), 95% confidence intervals (95% CI) of slope coefficients of *Idiognathodus* sp. and *G. bilineatus* were calculated according to the following formula:

$$\beta_1 = b_1 \pm t_{0.025,n-2} \times SE(b_1)$$

Where b_1 is the slope coefficient, n is the number of measurements, t is the t distribution and SE – standard error. Measurements for platform length of *G. bilineatus* were not available (Purnell 1994).

Quantitative topographic analysis (DNE)

Dirichlet Normal Energy (DNE) measures a surface's curvature and average sharpness (Bunn et al. 2011). The DNE of an object is independent of its size and orientation. Its equation is commonly written as follows:

$$DNE = \sum e(p) \times area(p)$$

Here, $e(p)$ is the Dirichlet Energy Density at a point p. The sum of the areas of all points p (however small) on a surface is equal to the total area of the surface. Flat planes have DNE values of 0. Therefore, a higher DNE value expresses the elements' complexity and the average "sharpness" of a surface (Bunn et al. 2011).

We applied the DNE on P_1 element meshes with the R package "molaR" 5.0 (Pampush et al. 2016). To ensure consistency of DNE calculation, all meshes were simplified to 10 000 faces (Spradley et al. 2017) using Quadric Edge Collapse Decimation in MeshLab. They were then rescaled so that each platform area equalled 0.1 mm^2. Meshes were then smoothed in Avizo using the Avizo smoothing function with lambda = 0.6 and 25 iterations. Twenty to thirty smoothing iterations, a conservative amount when compared to other approaches (Bunn et al.

2011; Winchester et al. 2014; Spradley et al. 2017), are recommended because they eliminate scanning noise while capturing fine-scale features and avoiding the creation of artificial dimples that can be caused by over smoothing (Spradley et al. 2017). Different numbers of iterations (5, 10, 15, 20, 25, 30, 40, 50, 60, 70, 80, 90, and 100) were tested on a single specimen of *M. communisti* to determine the impact of the number of smoothing iterations (Figure S2). The DNE appears stable from ~20 to 25 iterations.

The meshes were then manually cut to keep the occluding surface of the platform, the cusp and the postcarinal nodes (Figure 3). Additionally, we cut out the aboral part of the platform because it does not take actively part in the food processing. The meshes were finally imported into R Software as binary *ply* files. Individual pieces of meshes created by the smoothing operation were removed to prevent them from affecting the DNE calculation. DNE was calculated with an included boundary exclusion criterion (BoundaryDiscard="vertex"), as advised by Spradley et al. (2017). The total surface DNE is the mean of all DNE values for individual faces of a surface (Pampush et al. 2016). Reduced major axis regression (RMA) was used to examine the relationship between DNE and the length of the platform and between DNE and the platform area in both species. Growth stage 5 (GS5) was chosen to compare DNE values between species because this stage comprised enough specimens from both species to allow statistical analysis (Table 1). GS5, representing adults, also allows for interpretations of the diet. The DNE distributions were compared with a Kruskal-Wallis test in R (Hollander and Wolfe 1973).

The R code and data used for investigating allometric patterns and DNE are available on OSF at this address: https://osf.io/283wq/?view_only=6f22274998134eb99cbe43749c6e3e7e (Kelz et al. 2022).

Results

Growth allometry

In all examined relationships, high coefficients of determination ($R^2 \geq 0.89$) indicated that linear regression captured the relationships between the variables sufficiently (Table 2). In *Metapolygnathus communisti*, linear regression slopes of the platform length over the P_1 element length and of the platform area over the P_1 element length showed positive allometry (Figure 4A-B). In both cases the slopes differed significantly from values corresponding to isometry, i.e. one

and two, respectively (Table 2). No differences between the two ways the platform length was measured could be detected (p=0.23; Figure S1A).

In *Epigondolella rigoi*, both regression slopes (platform length over element length and platform area over element length) indicated positive allometry and were significantly higher than predicted under the null hypothesis of isometric growth (Table 2; Figure 4C-D). No significant difference between the two ways the platform length was measured could be detected (p=0.83; Figure S1B).

Slope coefficients of the platform length over element length did not differ significantly between *M. communisti* and *E. rigoi* (p=0.166), but in both cases they were significantly higher than that of *Idiognathodus* sp. as their confidence intervals did not overlap (Table 2, Figure 4E, G). Platform areas in all four species showed positive allometry over element length but at different rates: slope coefficients in *M. communisti* and *E. rigoi* were considerably higher than *Idiognathodus* sp. and *Gnathodus bilineatus* (2.561 and 2.392 *vs.* 2.149 and 2.164 respectively) but their 95% confident intervals overlapped and no significant difference was detected between *M. communisti* and *E. rigoi* (p=0.479). Thus, no significant differences could be detected between the slopes in these four taxa (Table 2, Figure 4F-G).

Dental topography (DNE)

In *M. communisti*, DNE values ranged between 99.93 and 279.84; in *E. rigoi*, between 117.59 and 353.71 (Figure 5). In *M. communisti* and *E. rigoi*, a positive linear relationship was detected between DNE values and platform length (Figure 5A, Table 3) and between DNE values and platform area (Figure 5B, Table 3). The regression slopes were supported by moderately high coefficients of determination ($0.500 \leq R^2 \leq 0.621$; Table 3). In either case no significant differences between the two species could be found (p=0.15 for DNE over platform length; p=0.23 for DNE over platform area).

Specimens classified as GS5 of *E. rigoi* showed higher DNE values than GS5 specimens of *M. communisti* (Kruskal-Wallis test, p=0.015; Figure 5C).

Discussion

Growth Allometry

The null hypothesis of an isometric growth of P_1 elements in *M. communisti* and *E. rigoi* could be rejected based on positive growth allometry of the platform length and platform area

over element length. These results support previous findings of positive growth allometry in these organs in much older, Carboniferous, ozarkodinid taxa *G. bilineatus* and *Idiognathodus* sp. (Purnell 1993, 1994). They are consistent with the interpretation of P_1 elements as organs used for mechanical slicing and grinding of food, as previously proposed based on microwear (Purnell 1995; Martínez-Pérez et al. 2014*b*), enamel-like ultrastructure of conodont lamellar crown tissue (Purnell et al. 2000), and finite element analysis (Jones et al. 2012*a*).

Our hypothesis that *M. communisti* and *E. rigoi* differed in the growth allometry of their P_1 elements as a reflection of occupying different trophic niches could not be rejected, as the difference in slopes was insignificant. Similar growth allometry might indicate similar trophic level, but different types of food processed within that level (see discussion of DNE results). Such partial overlaps of trophic niches of conodonts has been suggested in Silurian conodont communities based on geochemical proxies (Terrill et al. 2022).

Based on growth allometry implying platform length, we can reject the null hypothesis that Late Triassic species shared the same trophic position than the Carboniferous *Idiognathodus* sp. because their allometric slope coefficient differ significantly (Figure 4G). However, the same null hypothesis cannot be rejected considering the allometric growth of platform area. Indeed, 3D measurement of platform areas (*M. communisti* and *E. rigoi*) resulted in higher regression slopes, but the difference was not significant (Table 2, Figure 4A). Perhaps this insignificant difference in slope coefficient resulted in the methodological difference in platform area measurement between Purnell (1993, 1994) and us. Indeed, measurements based on pictures suffer from distortions resulting from projecting on a plane, where differences in levelling the photographed specimens might affect the results. Nevertheless, a proper 3D measurements of P_1 platform area using our methodological protocol should be investigated in *Idiognathodus* sp. specimens to verify if there is any difference in allometric slope coefficients. Then, we cannot be certain that Late Triassic and Carboniferous species shared or not the same trophic position. However, as platform length showed a stronger positive allometry in Late Triassic taxa than found in *Idiognathodus* sp, it suggests that the increase of functional surface was primarily achieved in these taxa by platform elongation, rather than growth in width. The cause(s) of this ontogenetic pattern is not resolved here and is beyond the scope of this study but future research on the development of conodont elements will help to understand it.

Platform sharpness

In *M. communisti* and *E. rigoi*, DNE values differed at the adult growth stage (i.e., GS5) and the values increased approximately linearly with both platform length and platform area. The hypothesis that the rate of DNE increase remained the same throughout ontogeny could not, therefore, be rejected (Figure 5). This indicates that platform complexity increased at comparable rate in both species, suggesting that their food base or energy use did not change as they grew. This is different from the observation made in Silurian conodonts that they may have had a different feeding strategy during their larval stage (Shirley et al. 2018).

We compared DNE values between *M. communisti* and *E. rigoi* based only on values on GS5 specimens because ontogenetically younger growth stages were represented by fewer specimens in both species (Table 1), which made observations of these stages less conclusive. A limitation of our analysis was that growth stages were differentiated based on morphology (i.e., size and presence/numbering of morphological characters), not sexual maturity. Thus, the classification of GS5 as "adult" does not consider biology, but the morphological maturity of the elements (Mazza and Martínez-Pérez 2015). However, GS5 is one of the more mature stages, so we can be confident on the maturity of the conodonts that bore these P_1 elements. Differences in DNE values between *M. communisti* and *E. rigoi* allow rejecting the hypothesis that both species shared the same diet. More DNE analyses on conodonts are needed to understand the scope of DNE values in this group and to confidently suggest that a discrepancy between DNE values of different species reflects different dietary niches. Indeed, DNE values of GS5 specimens of *M. communisti* are similar to those reported for folivores or omnivores; insectivores or folivores in the case of *E. rigoi*, but these diets based on DNE values stem from studies on primates (Bunn et al. 2011; Winchester et al. 2014). Moreover, conodont elements are more than ten time smaller than primate teeth, which complicate dietary comparison as conodonts could not eat exactly the same objects than primates. Though primate dietary classifications do not apply to conodonts, they may offer a general reference point for the methods of breaking down different food types. Insectivores rely on sharp cusps to apply maximal force to a small surface, to pierce hard insect chitin, and folivores also use steeply sloped cusps to shear tough cellulose-rich leaves (Lucas 1979; Strait 1997). It is possible that conodont element platforms evolved to break down food types with similar properties. For instance, conodonts may have punctured arthropod larvae (Dzik 2021), which would be consistent with the DNE values observed in *M. communisti*.

The definition of the platform for DNE measurement is worth discussing because it is somewhat subjective. In this work, we decided to include the cusp and all postcarinal nodes because, in many cases, the cusp marked a notable transition between sharper denticles of the blade and flatter nodes on the platform. In *M. communisti*, the number of postcarinal nodes increases through growth (Mazza et al. 2012*a*; Mazza and Martínez-Pérez 2015), impacting DNE values through the ontogeny of this species. In *E. rigoi*, the number of posterior nodes stays the same (Mazza et al. 2012*a*) so variations of DNE values are more related to the growth of prior postcarinal nodes or the addition of new nodes on the edge of the platform. This difference in nodes location on the platform might affect the way conodonts break down food and so their diet but it should be further investigated by assessing occlusal kinematics of *M. communisti* and *E. rigoi* P_1 elements, which is currently impossible because no clusters is currently known for these species.

There are several challenges researchers face when working with DNE in conodonts. As DNE is a comparatively new tool, reference values and understanding of variability (e.g. intraspecific, ontogenetic and resulting from preservation) are limited. So far, DNE research has focused on mammals, whose tooth function is, in large part, reliant on jaws acting as levers. The different mechanics of feeding in jawed organisms necessitates that the comparisons drawn here between conodont elements and primate molars must be viewed as extremely hypothetical. Marine environment, evolutionary distance and the lack of jaws in conodonts make tooth function likely not completely analogous between the two. Even more importantly, conodonts are unique among vertebrates in repairing their teeth by periodic apposition of new growth layers on top of the ones previously used for food processing. Thus, tooth morphology is expected to change periodically during the life of the animal and this might results in fluctuations of DNE values in function of the moment of the feeding season. Typical applications of DNE do not take into account ontogenetic development (see references above in the Introduction). However, contrary to mammalian molars, the number of denticles in P_1 element platforms increases during ontogenetic growth in conodonts. This variable morphology plays into the problem of what to include in the conodont platform, which also has an impact on the calculation and reproducibility of DNE. A consistent protocol of mesh preparation before DNE calculation is also needed. For example, the scan resolution and the number of smoothing iterations vary in current literature and this can impact DNE results (Spradley et al. 2017; Assemat et al. 2022). This variation in processing is

important because comparisons are most conclusive when drawn between data with similar preparation. We second the recommendations by Spradley et al. (2017): a conservative number of smoothing iterations (20-30) using non-Laplace-based smoothing operators, such as that implemented in Avizo, and mesh simplification to a fixed number of faces. About the scan resolution, it depends on the size of the studied object. We cannot expect a 1 µm resolution (as for conodont P_1 elements from the Pizzo Mondello (Guenser et al. 2019)), for mammal teeth of several mm in length. However, we can set a standardised scan resolution for conodonts elements of 1 µm (even lower would be better), which would allow investigating ontogenetic patterns by including P_1 elements of less than 400 µm in length (i.e., juveniles).

Previous investigations showed that dental topography methods could be applied to non-homologous dental tools to track dietary differences between distantly related clades (Stockey et al. 2021). Conodont elements in this study showed similar sharpness to complex mammal teeth. This similarity does not mean that direct dietary associations can be made between conodonts and mammals, but dental topography allows comparisons between taxa and ontogenetic stages and helps in constraining conodont ecology (Purnell and Evans 2009).

Conclusions

We used 3D meshes to test the null hypothesis that Late Triassic conodont P_1 elements grew isometrically. We tested it against the alternative hypothesis that they showed positive allometry, which would imply that they performed molar-like function. We followed Purnell's protocol (1993, 1994), analysing the growth allometry of the platform length and area *vs.* total length of the element, originally performed on 2D projections of conodont elements. We further used slopes of these allometric relationships to test the hypothesis that conodonts occupying the same environments shared the same trophic positions. Platform length and platform area showed positive allometry with respect to element length, allowing us to reject the null hypothesis in support of conodont growth consistent with molar-like function. Slope coefficients did not differ between *M. communisti* and *E. rigoi*. However, for platform length over element length slope coefficients were higher than those reported for Carboniferous conodonts *Idiognathodus* sp. (Purnell 1994). A more precise measurement of surface area in 3D models compared to 2D projections used in *Idiognathodus* sp. did not result in a significantly different relationship. In

contrast, length- rather than area-based measurements allowed detecting significant differences between Late Triassic taxa and *Idiognathodus* sp.

We added dental topographic analysis of the platforms using DNE to test the hypotheses that the diets of *M. communisti* and *E. rigoi* did not change during ontogenetic growth and that they occupied the same dietary niches. Surface DNE values increased linearly at the same rate as a function of element length and platform area, indicating no ontogenetic changes. *E. rigoi* specimens showed significantly higher DNE values than *M. communisti* specimens when comparing adult growth stages. Based on DNE values available for primates, those of the adult growth stages of *E. rigoi* were similar to those reported for insectivores or folivores, folivores or omnivores in the case of *M. communisti*.

Previous studies applying morphological and ultrastructural proxies for the dietary position of conodonts addressed mostly stratigraphically older conodont taxa, but our results indicate that Late Triassic species occupied the predator/scavenger niche. We also show that co-occurring taxa differed in their diets within this broad niche, which supports trophic diversification as an important driver of the remarkable disparity of their elements.

Acknowledgements

We thank Bryan Shirley for support in using Aviso and Wyatt Petryshen for advice on cleaning and saving meshes. We also thank Michele Mazza for advices and field sampling. We finally thank Nicolas Goudemand for supporting the project (French ANR grant, ACHN project EvoDevOdonto). PG was supported by Visiting Scholarship awarded by Friedrich-Alexander-Universität Erlangen-Nürnberg. EJ was supported by Deutsche Forschungsgemeinschaft (project no JA 2718/3-1). MR was supported by DOR2054230/20 by University of Padova. We are grateful to Viktor Karádi, Nicolas Campione and Paleobiology Editor James Crampton for constructive comments, which improved the manuscript.

Literature cited

Alberch, P., S. J. Gould, G. F. Oster, and D. B. Wake. 1979: Size and shape in ontogeny and phylogeny. Paleobiology 5:296–317.

Assemat, A., G. Thiery, T. Lieffroy, and C. Girard. 2022: 3D topography as tool for shape discrimination of conodont elements. Fifth International Conodont Symposium (ICOS5).

Balter, V., J. E. Martin, T. Tacail, G. Suan, S. Renaud, and C. Girard. 2019: Calcium stable isotopes place Devonian conodonts as first level consumers. Geochemical Perspectives Letters 10:36–39.

457 Bengtson, S. 1976: The structure of some Middle Cambrian conodonts, and the early evolution
458 of conodont structure and function. Lethaia 9:185–206.
459 Berthaume, M. A., and K. Schroer. 2017: Extant ape dental topography and its implications for
460 reconstructing the emergence of early Homo. Journal of Human Evolution 112:15–29.
461 Bunn, J. M., D. M. Boyer, Y. Lipman, E. M. St. Clair, J. Jernvall, and I. Daubechies. 2011:
462 Comparing Dirichlet normal surface energy of tooth crowns, a new technique of molar
463 shape quantification for dietary inference, with previous methods in isolation and in
464 combination. American Journal of Physical Anthropology 145:247–261.
465 Cignoni, P., M. Callieri, M. Corsini, M. Dellepiane, F. Ganovelli, and G. Ranzuglia. 2008:
466 Meshlab: an open-source mesh processing tool. Eurographics Italian Chapter Conference
467 2008:129–136.
468 Cuesta-Torralvo, E., D. Pacheco, L. M. Martínez, A. Romero, C. Umbelino, Y. Avià, and A.
469 Pérez-Pérez. 2021: Three-dimensional proxies to dental wear characterization in a known
470 age-at-death skeletal collection. Journal of Archaeological Method and Theory 28:1261–
471 1275.
472 Donoghue, P. C. J. 2001a: Conodonts meet cladistics: recovering relationships and assessing the
473 completeness of the conodont fossil record. Palaeontology 44:65–93.
474 ———. 2001b: Microstructural variation in conodont enamel is a functional adaptation.
475 Proceedings of the Royal Society of London. Series B: Biological Sciences 268:1691–
476 1698.
477 Donoghue, P. C. J., and M. A. Purnell. 1999a: Growth, function, and the conodont fossil record.
478 Geology 27:251–254.
479 ———. 1999b: Mammal-like occlusion in conodonts. Paleobiology 25:58–74.
480 Donoghue, P. C. J., M. A. Purnell, and R. J. Aldridge. 1998: Conodont anatomy, chordate
481 phylogeny and vertebrate classification. Lethaia 31:211–219.
482 Du, Y., M. Chiari, V. Karádi, A. Nicora, T. Onoue, J. Pálfy, G. Roghi, Y. Tomimatsu, and M.
483 Rigo. 2020: The asynchronous disappearance of conodonts: New constraints from
484 Triassic-Jurassic boundary sections in the Tethys and Panthalassa. Earth-Science
485 Reviews 203:103176.
486 Dzik, J. 1991: Evolution of oral apparatuses in the conodont chordates. Acta Palaeontologica
487 Polonica 36:265–323.
488 ———. 2008: Evolution of morphogenesis in 360-million-year-old conodont chordates
489 calibrated in days. Evolution & Development 10:769–777.
490 ———. 2015: Evolutionary roots of the conodonts with increased number of elements in the
491 apparatus. Earth and Environmental Science Transactions of the Royal Society of
492 Edinburgh 106:29–53.
493 ———. 2021: Protaspis larva of an aglaspidid-like arthropod from the Ordovician of Siberia and
494 its habitat. Arthropod Structure & Development 61:101026.
495 Epstein, A. G., J. B. Epstein, and L. D. Harris. 1977: Conodont color alteration: an index to
496 organic metamorphism. United States Geological Survey Professional Paper 995:1–27.
497 Foote, M., and J. J. Sepkoski. 1999: Absolute measures of the completeness of the fossil record.
498 Nature 398:415–417.
499 Fulwood, E. L. 2020: Ecometric modelling of tooth shape and precipitation gradients among
500 lemurs on Madagascar. Biological Journal of the Linnean Society 129:26–40.
501 Gabbott, S. E., R. J. Aldridge, and J. N. Theron. 1995: A giant conodont with preserved muscle
502 tissue from the Upper Ordovician of South Africa. Nature 374:800–803.

Ginot, S., and N. Goudemand. 2019: Conodont size, trophic level, and the evolution of platform elements. Paleobiology 45:458–468.

Godfrey, L. R., J. M. Winchester, S. J. King, D. M. Boyer, and J. Jernvall. 2012: Dental topography indicates ecological contraction of lemur communities. American Journal of Physical Anthropology 148:215–227.

Goudemand, N., M. J. Orchard, S. Urdy, H. Bucher, and P. Tafforeau. 2011: Synchrotron-aided reconstruction of the conodont feeding apparatus and implications for the mouth of the first vertebrates. Proceedings of the National Academy of Sciences 108:8720–8724.

Gould, S. J. 1966: Allometry and size in ontogeny and phylogeny. Biological Reviews 41:587–638.

Guenser, P., L. Souquet, S. Dolédec, M. Mazza, M. Rigo, and N. Goudemand. 2019: Deciphering the roles of environment and development in the evolution of a Late Triassic assemblage of conodont elements. Paleobiology 45:440–457.

Harper, T., A. Parras, and G. W. Rougier. 2019: *Reigitherium* (Meridiolestida, Mesungulatoidea) an enigmatic Late Cretaceous mammal from Patagonia, Argentina: morphology, affinities, and dental evolution. Journal of Mammalian Evolution 26:447–478.

Hayami, I., and A. Matsukuma. 1970: Variation of bivariate characters from the standpoint of allometry. Palaeontology 13:588–605.

Hayashi, S. 1968: The Permian conodonts in chert of the Adoyama Formation, Ashio Mountains, central Japan. Earth Science 2:63–77.

Hollander, M., and D. A. Wolfe. 1973: Nonparametric statistical methods. Vol. 751. John Wiley & Sons, p.

Jones, D., A. R. Evans, E. J. Rayfield, K. K. W. Siu, and P. C. J. Donoghue. 2012a: Testing microstructural adaptation in the earliest dental tools. Biology Letters 8:952–955.

Jones, D., A. R. Evans, K. K. W. Siu, E. J. Rayfield, and P. C. J. Donoghue. 2012b: The sharpest tools in the box? Quantitative analysis of conodont element functional morphology. Proceedings of the Royal Society B: Biological Sciences 279:2849–2854.

Kelz, V., P. Guenser, M. Rigo, and E. Jarochowska. 2022: Growth allometry and dental topography in Upper Triassic conodonts support trophic differentiation and molar-like element function. Dataset retrieved from osf.io/283wq. .

Klingenberg, C. P. 1996: Multivariate Allometry. Pp.23–49 *in* L. F. Marcus, M. Corti, A. Loy, G. J. P. Naylor, and D. E. Slice, eds. Advances in Morphometrics. Springer US, Boston, MA.

Klug, C., B. Kröger, W. Kiessling, G. L. Mullins, T. Servais, J. Fryda, D. Korn, and S. Turner. 2010: The Devonian nekton revolution. Lethaia 43:465–477.

Lang, A. J., T. Engler, and T. Martin. 2022: Dental topographic and three-dimensional geometric morphometric analysis of carnassialization in different clades of carnivorous mammals (Dasyuromorphia, Carnivora, Hyaenodonta). Journal of Morphology 283:91–108.

Li, P., P. E. Morse, and R. F. Kay. 2020: Dental topographic change with macrowear and dietary inference in *Homunculus patagonicus*. Journal of Human Evolution 144:102786.

López-Aguirre, C., S. J. Hand, N. B. Simmons, and M. T. Silcox. 2022: Untangling the ecological signal in the dental morphology in the bat superfamily Noctilionoidea. Journal of Mammalian Evolution.

López-Torres, S., K. R. Selig, K. A. Prufrock, D. Lin, and M. T. Silcox. 2018: Dental topographic analysis of paromomyid (Plesiadapiformes, Primates) cheek teeth: more than

15 million years of changing surfaces and shifting ecologies. Historical Biology 30:76–88.

Lucas, P. W. 1979: The Dental-Dietary Adaptations of Mammals. Neues Jahrbuch für Geologie und Paläontologie Monatshefte 8:486–512.

Martínez-Pérez, C., E. J. Rayfield, M. A. Purnell, and P. C. J. Donoghue. 2014a: Finite element, occlusal, microwear and microstructural analyses indicate that conodont microstructure is adapted to dental function. Palaeontology 57:1059–1066.

Martínez-Pérez, C., E. J. Rayfield, H. Botella, and P. C. J. Donoghue. 2016: Translating taxonomy into the evolution of conodont feeding ecology. Geology 44:247–250.

Martínez-Pérez, C., P. Plasencia, D. Jones, T. Kolar-Jurkovšek, J. Sha, H. Botella, and P. C. J. Donoghue. 2014b: There is no general model for occlusal kinematics in conodonts. Lethaia 47:547–555.

Mazza, M., and C. Martínez-Pérez. 2015: Unravelling conodont (Conodonta) ontogenetic processes in the Late Triassic through growth series reconstructions and X-ray microtomography. Bollettino della Società Paleontologica Italiana 54:161–186.

Mazza, M., M. Rigo, and M. Gullo. 2012a: Taxonomy and biostratigraphic record of the Upper Triassic conodonts of the Pizzo Mondello section (western Sicily, Italy), GSSP candidate for the base of the Norian. Rivista Italiana di Paleontologia e Stratigrafia 118:85–130.

Mazza, M., A. Cau, and M. Rigo. 2012b: Application of numerical cladistic analyses to the Carnian–Norian conodonts: a new approach for phylogenetic interpretations. Journal of Systematic Palaeontology 10:401–422.

Mazza, M., A. Nicora, and M. Rigo. 2018: *Metapolygnathus parvus* Kozur, 1972 (Conodonta): a potential primary marker for the Norian GSSP (Upper Triassic). Bollettino della Società Paleontologica Italiana.

Mazza, M., S. Furin, C. Spötl, and M. Rigo. 2010: Generic turnovers of Carnian/Norian conodonts: Climatic control or competition? Palaeogeography, Palaeoclimatology, Palaeoecology 290:120–137.

Miyashita, T., Coates Michael I., Farrar Robert, Larson Peter, Manning Phillip L., Wogelius Roy A., Edwards Nicholas P., Anné Jennifer, Bergmann Uwe, Palmer A. Richard, and Currie Philip J. 2019: Hagfish from the Cretaceous Tethys Sea and a reconciliation of the morphological–molecular conflict in early vertebrate phylogeny. Proceedings of the National Academy of Sciences 116:2146–2151.

Nicoll, R. S. 1987: Form and function of the Pa element in the conodont animal. Pp.77–90 *in* R. J. Aldridge, ed. Palaeobiology of Conodonts. Ellis Horwood, Chichester.

Nicora, A., M. Balini, A. Bellanca, A. Bertinelli, S. A. Bowring, P. Di Stefano, P. Dumitrica, C. Guaiumi, M. Gullo, A. Hungerbuehler, and others. 2007: The Carnian/Norian boundary interval at Pizzo Mondello (Sicani Mountains, Sicily) and its bearing for the definition of the GSSP of the Norian Stage. Albertiana 36:102–129.

Noyan, Ö. F., and H. W. Kozur. 2007: Revision of the late Carnian–early Norian conodonts from the Stefanion section (Argolis, Greece) and their palaeobiogeographic implications. Neues Jahrbuch für Geologie und Paläontologie-Abhandlungen 245:159–178.

Ogg, J. G., Z.-Q. Chen, M. J. Orchard, and H. S. Jiang. 2020: Chapter 25 - The Triassic Period. Pp.903–953 *in* F. M. Gradstein, J. G. Ogg, M. D. Schmitz, and G. M. Ogg, eds. Geologic Time Scale 2020. Elsevier.

592 Pampush, J. D., J. M. Winchester, P. E. Morse, A. Q. Vining, D. M. Boyer, and R. F. Kay. 2016:
593 Introducing molaR: a New R Package for Quantitative Topographic Analysis of Teeth
594 (and Other Topographic Surfaces). Journal of Mammalian Evolution 23:397–412.
595 Pampush, J. D., J. Crowell, A. Karme, S. A. Macrae, R. F. Kay, and P. S. Ungar. 2019:
596 Technical note: Comparing dental topography software using platyrrhine molars.
597 American Journal of Physical Anthropology 169:179–185.
598 Pellegrom, C. 2019: Dental topographic analysis of maxillary and mandibular phyllostomid bat
599 dentitions: implications for dietary prediction in the fossil record. Masters Theses.
600 Pérez-Ramos, A., A. Romero, E. Rodriguez, and B. Figueirido. 2020: Three-dimensional dental
601 topography and feeding ecology in the extinct cave bear. Biology Letters 16:20200792.
602 Petryshen, W., C. M. Henderson, K. De Baets, and E. Jarochowska. 2020: Evidence of parallel
603 evolution in the dental elements of Sweetognathus conodonts. Proceedings of the Royal
604 Society B: Biological Sciences 287:20201922.
605 Prufrock, K. A., S. López-Torres, M. T. Silcox, and D. M. Boyer. 2016: Surfaces and spaces:
606 troubleshooting the study of dietary niche space overlap between North American stem
607 primates and rodents. Surface Topography: Metrology and Properties 4:024005.
608 Purnell, M. A. 1993: Feeding mechanisms in conodonts and the function of the earliest
609 vertebrate hard tissues. Geology 21:375–377.
610 ———. 1994: Skeletal ontogeny and feeding mechanisms in conodonts. Lethaia 27:129–138.
611 ———. 1995: Microwear on conodont elements and macrophagy in the first vertebrates. Nature
612 374:798–800.
613 Purnell, M. A., and P. H. von Bitter. 1992: Blade-shaped conodont elements functioned as
614 cutting teeth. Nature 359:629–631.
615 Purnell, M. A., and A. Evans. 2009: Conodont tooth complexity: quantification, convergence
616 with mammals, and implications for dietary analysis. 53:39–40.
617 Purnell, M. A., P. C. J. Donoghue, and R. J. Aldridge. 2000: Orientation and anatomical notation
618 in conodonts. Journal of Paleontology 74:113–122.
619 R Core Team. 2021: R: a language and environment for statistical computing. R Foundation for
620 Statistical Computing, Vienna, Austria.
621 Rannikko, J., H. Adhikari, A. Karme, I. Žliobaitė, and M. Fortelius. 2020: The case of the grass-
622 eating suids in the Plio-Pleistocene Turkana Basin: 3D dental topography in relation to
623 diet in extant and fossil pigs. Journal of Morphology 281:348–364.
624 Renaud, S., and R. Ledevin. 2017: Impact of wear and diet on molar row geometry and
625 topography in the house mouse. Archives of Oral Biology 81:31–40.
626 Robson, S. V. 2018: An analysis of North American taeniolabidoid multituberculate (Mammalia,
627 Allotheria) dentitions using mammalian dietary proxies.Masters Theses, University of
628 Calgary, Calgary, Albertapp.
629 Schmidt, H. 1934: Conodonten-Funde in ursprünglichem Zusammenhang. Palaeontologische
630 Zeitschrift 16:76–85.
631 Scott, H. W. 1934: The zoological relationships of the conodonts. Journal of Paleontology
632 8:448–455.
633 Selig, K. R., S. López-Torres, E. J. Sargis, and M. T. Silcox. 2019: First 3D dental topographic
634 analysis of the enamel-dentine junction in non-primate euarchontans: contribution of the
635 enamel-dentine junction to molar morphology. Journal of Mammalian Evolution 26:587–
636 598.

637 Shirley, B., M. Grohganz, M. Bestmann, and E. Jarochowska. 2018: Wear, tear and systematic
638 repair: testing models of growth dynamics in conodonts with high-resolution imaging.
639 Proceedings of the Royal Society B: Biological Sciences 285:20181614.
640 Spradley, J. P., J. D. Pampush, P. E. Morse, and R. F. Kay. 2017: Smooth operator: The effects
641 of different 3D mesh retriangulation protocols on the computation of Dirichlet normal
642 energy. American Journal of Physical Anthropology 163:94–109.
643 Stockey, C., P. C. J. Donoghue, T. H. P. Harvey, D. J. E. Murdock, and M. A. Purnell. 2021:
644 Multivariate dental topographic metrics demonstrate the dietary breadth and specialisms
645 of conodonts. :46–47.
646 Stockey, C., P. C. . J. Donoghue, T. H. P. Harvey, D. J. E. Murdock, and M. A. Purnell. 2022:
647 Multivariate dental topographic metrics demonstrate the dietary breadth and specialisms
648 of conodonts. .
649 Strait, S. G. 1997: Tooth use and the physical properties of food. Evolutionary Anthropology:
650 Issues, News, and Reviews 5:199–211.
651 Terrill, D. F., E. Jarochowska, C. M. Henderson, B. Shirley, and O. Bremer. 2022: Sr/Ca and
652 Ba/Ca ratios support trophic partitioning within a Silurian conodont community from
653 Gotland, Sweden. Paleobiology:1–21.
654 Vermeer, H. 2019: The association between dietary niche variation in rodents and climate
655 change across the Paleocene-Eocene Thermal Maximum.Masters Theses, Grand Valley
656 State Universitypp.
657 Villalobos-Chaves, D., and S. E. Santana. 2022: Craniodental traits predict feeding performance
658 and dietary hardness in a community of Neotropical free-tailed bats (Chiroptera:
659 Molossidae). Functional Ecology 36:1690–1699.
660 Vitek, N. S., P. E. Morse, D. M. Boyer, S. G. Strait, and J. I. Bloch. 2021: Evaluating the
661 responses of three closely related small mammal lineages to climate change across the
662 Paleocene–Eocene thermal maximum. Paleobiology 47:464–486.
663 de Vries, D., S. Heritage, M. R. Borths, H. M. Sallam, and E. R. Seiffert. 2021: Widespread loss
664 of mammalian lineage and dietary diversity in the early Oligocene of Afro-Arabia.
665 Communications Biology 4:1172.
666 Warton, D. I., R. A. Duursma, D. S. Falster, and S. Taskinen. 2012: smatr 3– an R package for
667 estimation and inference about allometric lines. Methods in Ecology and Evolution
668 3:257–259.
669 Winchester, J. M., D. M. Boyer, E. M. St. Clair, A. D. Gosselin-Ildari, S. B. Cooke, and J. A.
670 Ledogar. 2014: Dental topography of platyrrhines and prosimians: Convergence and
671 contrasts. American Journal of Physical Anthropology 153:29–44.
672 Zhang, S., R. J. Aldridge, and P. C. J. Donoghue. 1997: An Early Triassic conodont with
673 periodic growth? J. Micropalaeontol. 16:65–72.
674 Zhang, Z. T., Y. D. Sun, P. B. Wignall, J. L. Fu, H. X. Li, M. Y. Wang, and X. L. Lai. 2018:
675 Conodont size reduction and diversity losses during the Carnian Humid Episode in SW
676 China. Journal of the Geological Society 175:1027–1031.

677

678 ## Table captions

679 Table 1: Numbers of conodont P1 element specimens by growth stages used for the study.

680 Abbreviations: GS – Growth stage.

	Metapolygnathus communisti	*Epigondolella rigoi*
GS2	0	1
GS3	3	1
GS4	2	6
GS5	7	15
GS6	15	0

681

682 Table 2: Linear regressions for platform length and platform area over element length for
683 Metapolygnathus communisti, Epigondolella rigoi, Idiognathodus sp. and Gnathodus bilineatus.
684 Data for Idiognathodus sp. and G. bilineatus were extracted from Purnell (1994) except for the
685 95% confidence intervals (CI). Slope coefficients and R^2 result from Reduced Major Axis
686 method. 95% CI values resulting from "sma" function calculation for M. communisti and E.
687 rigoi; from calculation for Idiognathodus sp. and G. bilineatus. The p-value results from the
688 "slope.test" function that compared the coefficients between species and isometry for M.
689 communisti and E. rigoi; from Z test (Hayami and Matsukuma 1970) for Idiognathodus sp. and
690 G. bilineatus.

Regression model	Species	Slope	Slope 95% CI lower value	Slope 95% CI upper value	R^2	p-value (h_0 = isometric growth)
PF length over element length	*Metapolygnathus communisti*	1.580	1.402	1.781	0.92	1.740×10^{-8}
	Epigondolella rigoi	1.403	1.238	1.590	0.92	1.101×10^{-5}
	Idiognathodus sp.	1.089	1.011	1.167	0.98	2.345 (Z test)
PF area over element length	*Metapolygnathus communisti*	2.561	2.230	2.940	0.89	1.039×10^{-3}
	Epigondolella rigoi	2.392	2.080	2.750	0.90	1.443×10^{-2}
	Idiognathodus sp.	2.149	2.002	2.296	0.98	2.060 (Z test)
	Gnathodus bilineatus	2.164	2.020	2.308	0.98	2.329 (Z test)

691

Table 3: Linear regressions for DNE values over element length and platform area for Metapolygnathus communisti and Epigondolella rigoi. Slope coefficients and R^2 result from the Reduced Major Axis method. 95% CI values resulting from "sma" function calculation. The p-value results from the "slope.test" function that compared the coefficients between species and isometry.

Regression model	Species	Slope	Slope CI lower value	Slope CI upper value	R^2	p-value (h0 = isometric growth)
DNE over platform length	*Metapolygnathus communisti*	122.566	94.848	158.386	0.62	0
	Epigondolella rigoi	163.819	120.195	223.275	0.52	0
DNE over platform area	*Metapolygnathus communisti*	75.411	58.210	97.696	0.61	0
	Epigondolella rigoi	96.121	70.102	131.797	0.50	0

Figure captions

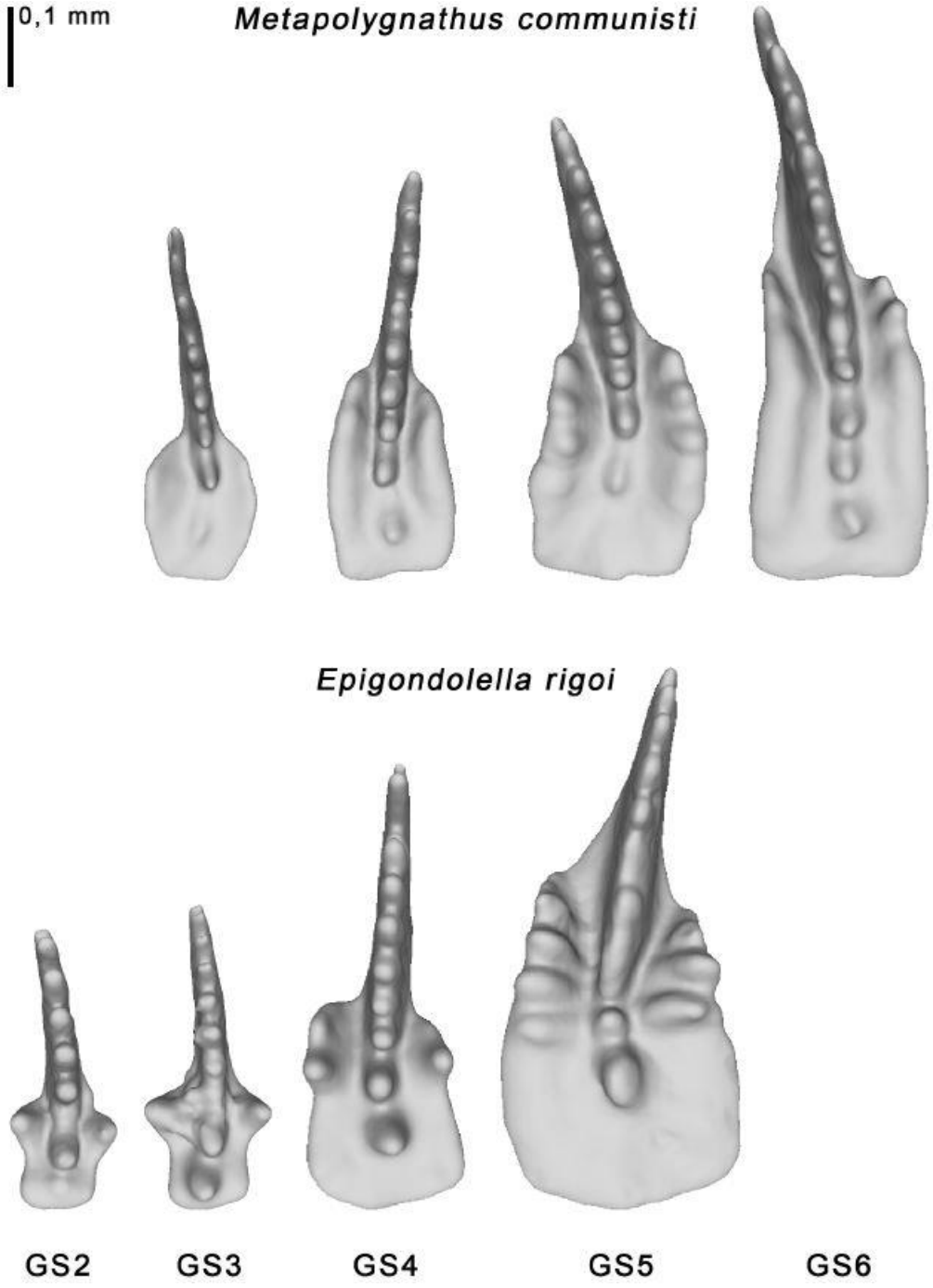

Figure 1: Growth stages of *Metapolygnathus communisti* and *Epigondolella rigoi*. For *M. communisti*: **GS3** – specimen NA37_18; **GS4** – specimen NA37_12; **GS5** – specimen NA37_01; **GS6** – specimen NA37_24. For *E. rigoi*: **GS2** – specimen NA59_20; **GS3** – specimen NA59_19; **GS4** – specimen NA59_01; **GS5** – specimen NA59_05.

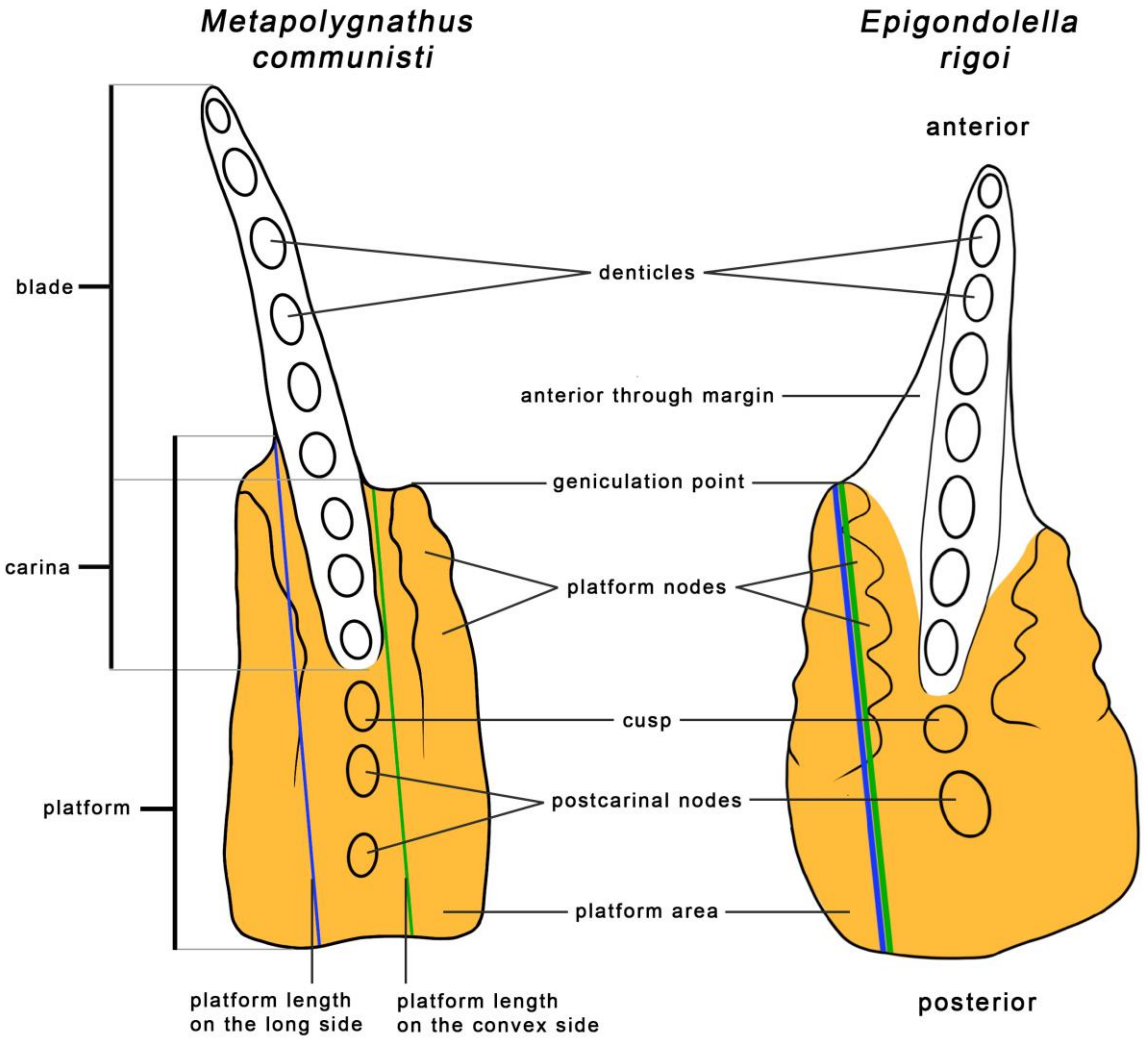

704

705 Figure 2: Measurements and morphological characters of P_1 elements illustrated on

706 *Metapolygnathus communisti* specimen NA37_24 and *Epigondolella rigoi* specimen NA59_05.

707 In most cases the convex side is also the long side. Morphological characters follow Mazza et al.

708 (2012*a*, *b*).

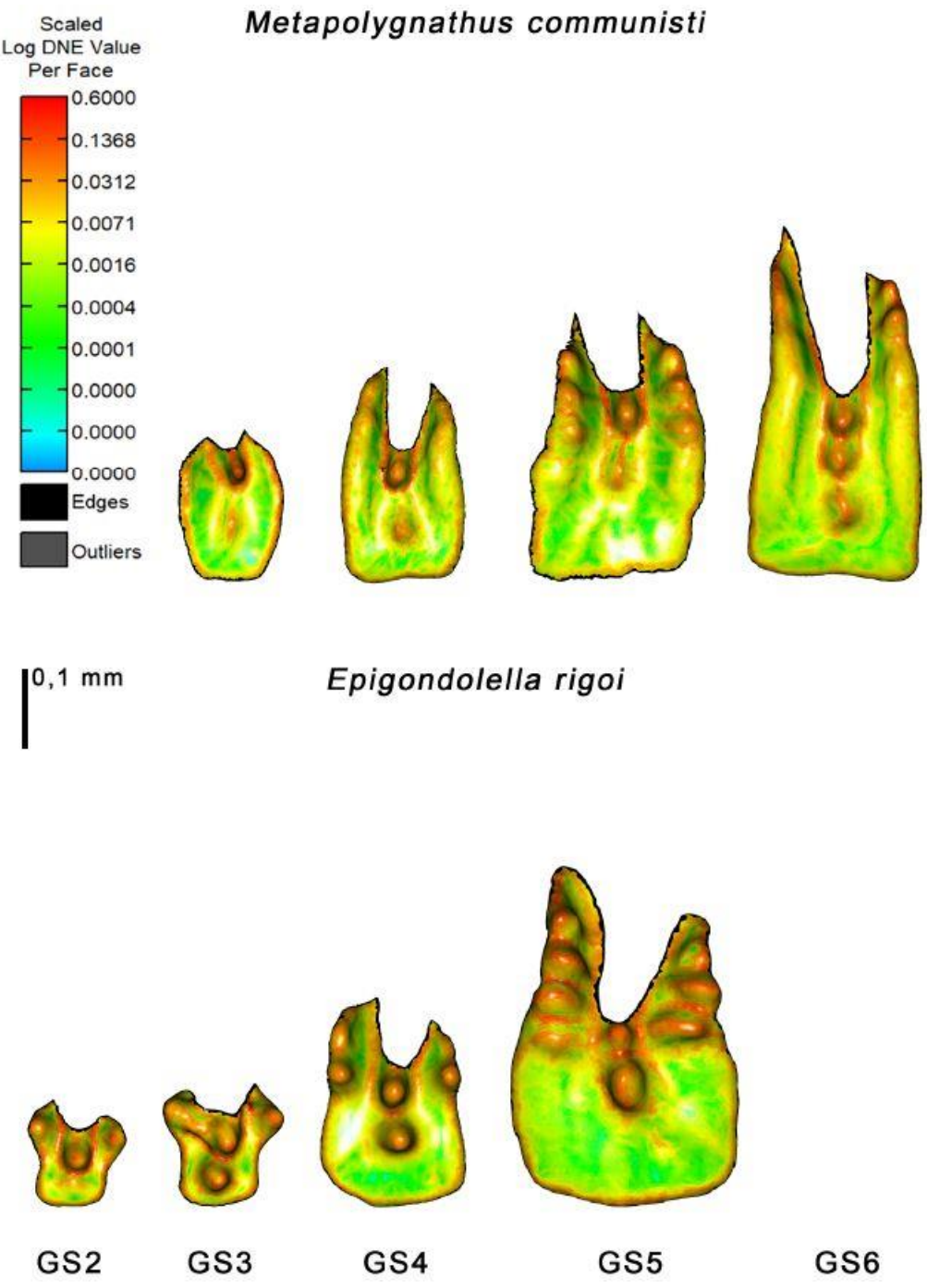

Figure 3: Log-transformed DNE values across growth stages GS3 to GS6 of *Metapolygnathus communisti* and across growth stages GS2 to GS5 of *Epigondolella rigoi*. Names of the specimens are specified in Figure 1.

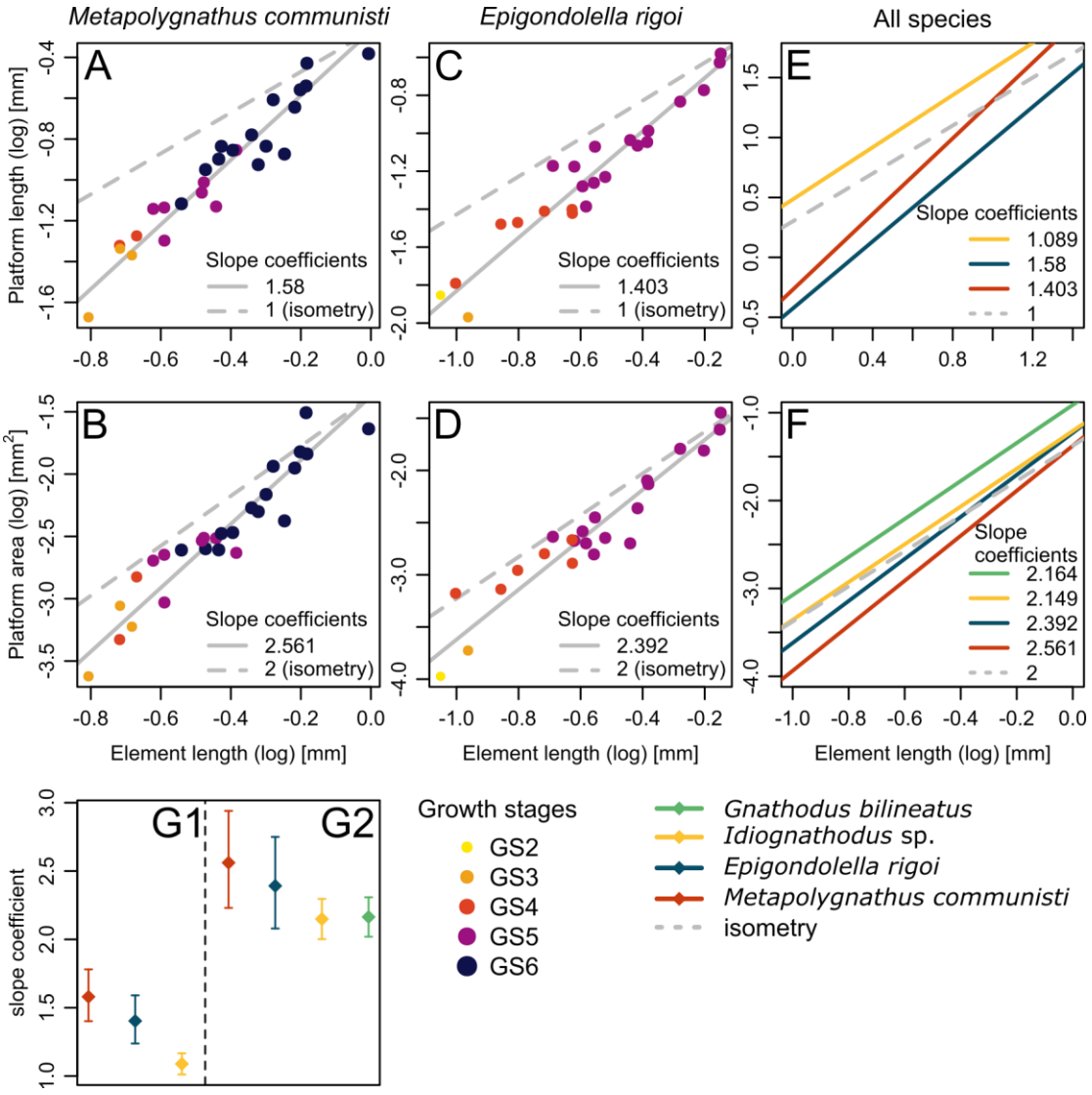

Figure 4: **A-D.** Allometric growth of P_1 platform length and P_1 platform area for *Metapolygnathus communisti* (n=27) and *Epigondolella rigoi* (n=23); each dot represents an element and the colours are related to the growth stage. **A.** Platform length over element length for *M. communisti*; convex platform length only. **B.** Platform area over element length for *M. communisti*. **C.** Platform length over element length for *E. rigoi*; convex platform length only. **D.** Platform area over element length for *E. rigoi*. **E-F.** Comparison of the allometric growth between *Gnathodus bilineatus* (Purnell 1994), *Idiognathodus* sp. (Purnell 1993, 1994), *E. rigoi* and *M. communisti*. **E.** Platform length over element length. Platform length in *M. communisti* and *E. rigoi* was measured on the convex side. No data were available for *G. bilineatus* (Purnell 1994). **F.** Platform area over element length. **G1-2.** Comparison of slope coefficients between species; G1, Platform length over element length; G2, platform area over element length.

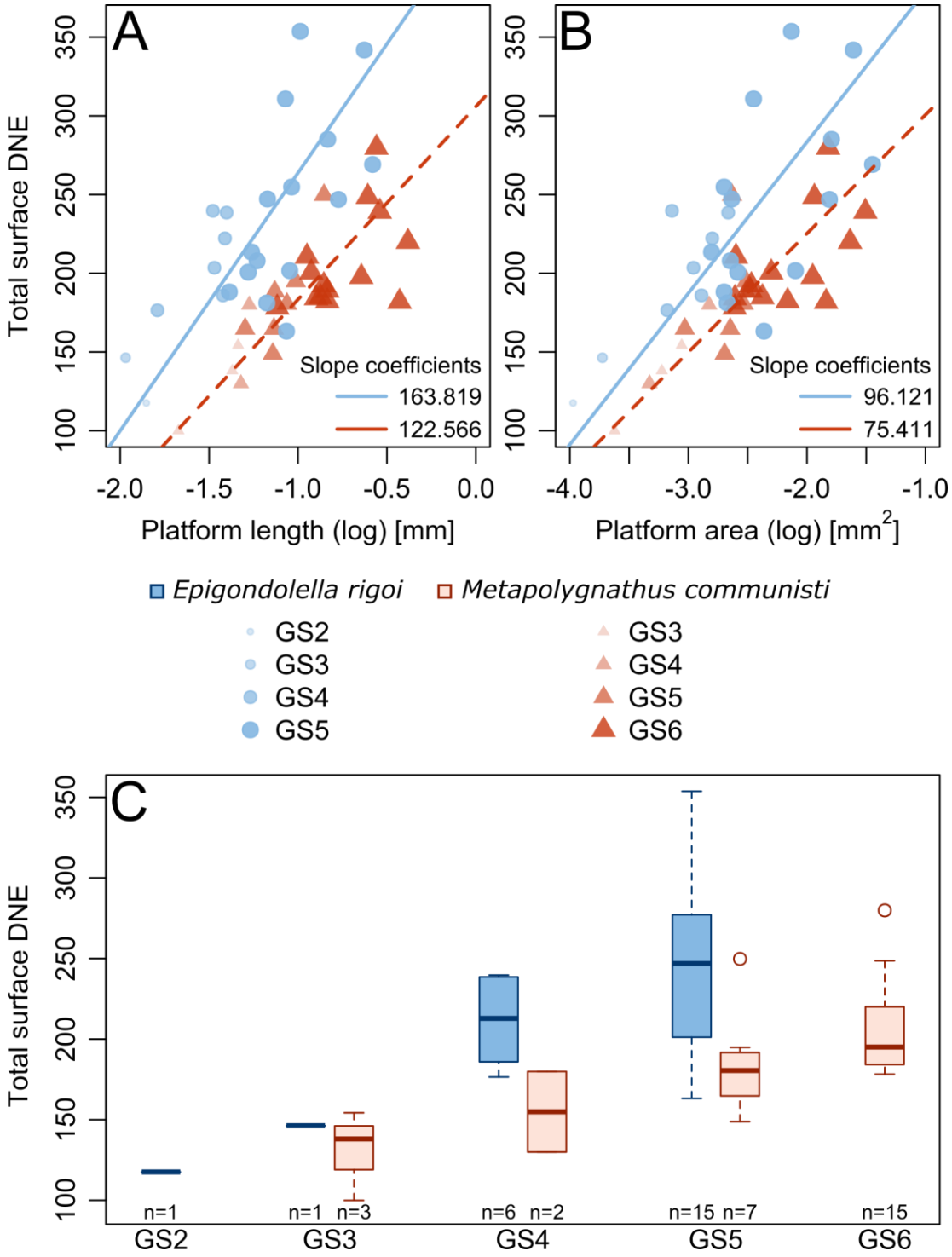

Figure 5: **A.** Regression of total surface DNE values over platform length in P_1 elements of *Epigondolella rigoi* and *Metapolygnathus communisti*. **B.** Regression of total surface DNE values over platform area in P_1 elements of *E. rigoi* and *M. communisti*. **C.** Distribution of DNE values across growth stages in *E. rigoi* and *M. communisti*.